postprint: Langmans, J., Nicolai, A., Klein, R., Roels, S. (2012). A quasi-steady state implementation of air convection in a transient heat and moisture building component model. Building and Environment, 58 (12), 208-218.

A quasi-steady state implementation of air convection in a transient heat and moisture building component model

Jelle Langmans[a*], Andreas Nicolai[b], Ralf Klein[c], Staf Roels[a]

[a] *Department of Civil Engineering, Building Physics Section, KU Leuven*
Kasteelpark Arenberg 40 - bus 02447, BE-3001 Heverlee, Belgium
[b] *Instituts fur Bauklimatik, Technical University of Dresden*
Zellescher Weg 17, 01069 Dresden, Germany
[c] *Sustainable Building Research Group, Departement of Industrial Engineering, Catholic University College Sint-Lieven*
G Desmetstraat 1, BE-9000 Ghent, Belgium

[*] *Corresponding author. Tel: +32 16 321348; fax: + 32 16 32 19 80*
E-mail address: jelle.langmans@bwk.kuleuven.be (J. Langmans)

Keywords: HAM, air convection, numerical simulation model, building component, buoyancy

Abstract

For many years, the coupled heat, air, and moisture (HAM) transport through multilayered building components has been an important research topic. As a result, a great number of numerical simulation tools have been developed to asses and predict the hygrothermal behaviour of building enclosures. But, while the literature shows the significant influence of air transport on the heat and moisture response of light weight constructions, only few existing heat and moisture transport models include air flow as an active mass component. One of the reasons is the different time scale of air transport compared to the other transported quantities and the resulting difficulties in achieving acceptable simulation performance.
The current article presents a quasi-steady state airflow model implementation in an existing transient HAM-model. The air transport is described as Darcy flow in porous media including a body force term to capture natural convection. One particular aim is the prediction of significant effects such as overlaying buoyant and externally driven air flow on the hygrothermal behaviour of building envelope components with sound simulation performances. Furthermore, the article includes an evaluation of the model. Therefore, three validation cases from the literature are used to show the applicability and limitations of the presented approach.

Nomenclature

Subscripts

a	air
atm	atmospheric
$cond$	conduction
$conv$	convection
d	dry air
$diff$	diffusion
lw	long wave
$rain$	rain
sw	short wave
v	water vapour
w	liquid water

Symbols

α	absorption coefficient $(-)$
α	heat transfer coefficient $(W/m^2/K)$
β	thermal expansion coefficient$(1/K)$
β	vapour transfer coefficient (s/m)
δ	vapour permeability (s)
$\dot{u}$	heat source (W/m^3)
η	dynamic viscosity $(Pa.s)$
λ	thermal conductivity $(W/m/K)$
μ	vapour resistance factor $(-)$
ν	kinetic viscosity (m^2/s)
ϕ	relative humidity $(\%)$
ρ	density (kg/m^3)
σ	ratio material heat capacity to fluids heat capacity $(-)$
τ	non-dimensional time $(-)$
θ	temperature $(^\circ C)$
φ	open porosity (m^3/m^3)
a	anisotropy ratio $(-)$
c	heat capacity $(J/kg/K)$
g	gravity force (m/s^2)
h	specific enthalpy (J/kg)
H_{evap}	evaporation enthalpy (J/kg)
j	mass flux $(kg/m^2/s)$
K	conductivity (s)
k	air permeability (m^2)
Nu	Nusselt number$(-)$
p	pressure(Pa)
q	energy flux (W/m^2)
R	gas constant $(J/(kg.K))$
Ra	Rayleigh number $(-)$
T	temperature (K)
t	time (s)
v	seepage velocity (m/s)
Re	Reynolds number (-)

1 Introduction

Moisture induced damage is one of the major causes of degradations and reduced thermal performance in building components. As a result, the coupled heat, air and moisture transport through building envelopes has been an important research topic for many years. Since experimental investigations are rather time consuming and expensive, a great number of numerical simulation tools have been developed over the years to asses and predict the hygrothermal behaviour of building components, mostly focusing on the heat and moisture transport [e.g. 1–5]. The existing HAM-models differ from each other by various assumptions in both the physical description and numerical implementation. An important step in standardising the various HAM-modelling procedures was made by the EU-initiated HAMSTAD-project (Heat, Air and Moisture Standards Development) [6]. Apart from suggesting useful benchmark cases this project concludes on the physical equations describing the combined heat, air and moisture transport in multilayered porous building components. However, the main emphasis of the HAMSTAD-project is on a detailed description of heat and moisture transport. Air transport is only briefly included and treated as a one-dimensional phenomenon.

Although most of today's hygrothermal building component modelling is focussing on heat and moisture transfer, the literature shows that air convection can highly influence its behaviour. Already from the 1960's onwards *in-situ* and experimental investigations identified natural and forced convection as one the most important sources of moisture problems and premature building component failure [e.g. 7–12]. As an example, Figure 1 presents the measured moisture content of the exterior sheathing of three different light weight walls exposed to Belgium climate conditions [12]. Apart from the interior lining the three walls were identically built. The left wall had a vapour retarding interior lining, the middle was vapour tight and the right wall was executed with a vapour open material. The interior layer of the left wall was perforated before the second winter resulting in forced exfiltration conditions from then on. The figure shows that this situation results in increased moisture content levels which are more than two times higher than the first winter. Furthermore, the figure also shows differences in the moisture content over the height of the walls (left and right walls) indicating the effect of natural convection.

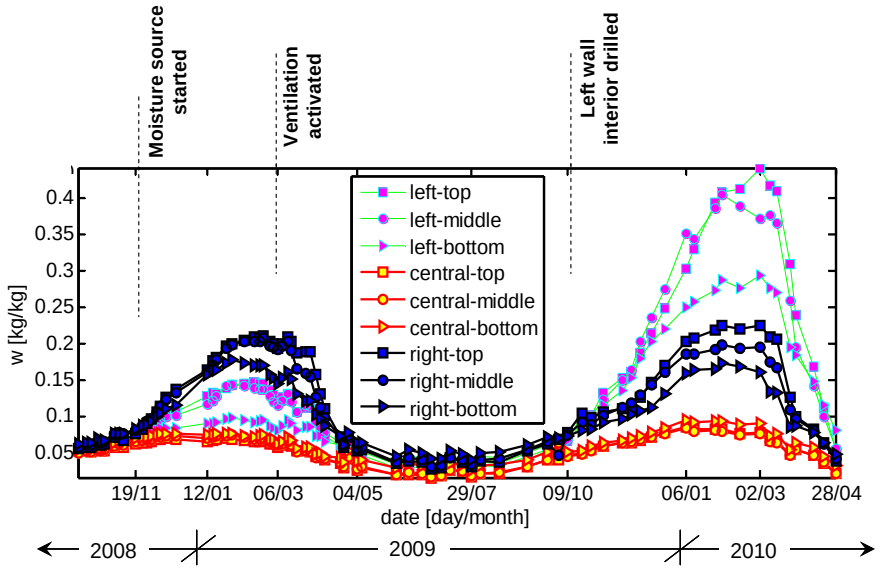

Figure 1: Measured moisture content evolution of the removable weight specimens in the exterior fibreboard sheathing [12]

Notwithstanding that the importance of air transport is documented in the literature, only few existing HAM-models include air as an active mass component. And if so, also the level of complexity that is used to describe air transport ranges from *a*) including the effect of the air transport on the moisture balance via a source term [e.g. 13], to *b*) a coupled or decoupled air mass balance including forced convection [e.g. 6], up to *c*) a coupled air mass balance including both natural and forced convection [e.g. 9, 14, 15]. Fully coupled models including this last approach combined with detailed heat, vapour and liquid moisture transport are scarce. Only a few specialised research-level simulation codes tailored to solve specific problem scenarios such as [4, 16–18] exist today. Most of these recent models use commercial simulation engines such as MATLAB-Simulink and COMSOL-Multiphysics. As a result of the large difference of the time scales between air transport and heat and moisture transport, the numerical stability or accuracy constraints of these general purpose solvers will usually result in extremely small time steps. As a consequence this leads to

excessive simulation times and essentially render these methods unsuitable for long-term simulations of general cases. In the field of computational fluid dynamics (CFD) on the other hand, the simulation of ventilated cavities including buoyancy and various boundary condition scenarios is state-of-the-art. However, such tools usually ignore the specifics of porous media modelling, and do not provide the means for applying boundary condition scenarios, such as radiation and wind driven rain, needed for building envelope simulations. Also, the computational speed of CFD simulations is generally not acceptable for long-term simulations of building enclosures. Recent attempts to couple the fluid and porous domain such as [19, 20] still assume airtight porous media.

The current article presents a modelling and simulation approach that tries to bridge the accuracy requirements with acceptable solver performance. The major aim of the method described in this paper is to present an accurate scheme with an acceptable simulation time that can be used to evaluate the hygrothermal performance of building components. A steady-state air mass balance equation is solved together with a transient energy and moisture balance equation. The calculation domain consists of porous materials in which the air transport is treated as Darcy flow. A staggered calculation method is presented to solve the given set of differential-algebraic equations (DAE). The heat and moisture balance equation are solved with a state-of-the-art ordinary differential equation (ODE)-solver, while the air mass balance equation is solved separately at given intervals using the current heat and moisture conditions. After the description of the modelling strategy the current article focusses on the evaluation and applicability of the model. In a first step the coupling between the heat and air balance equations is evaluated by simulating analytical and numerical results from the literature. In a second step the results of the present model are compared with a full scale laboratory investigation studying the impact of air convection on the hygrothermal behaviour of a timber frame wall.

2 Principle Model Equations

The current article shows the implementation and evaluation of air transport in the existing simulation package DELPHIN developed at the Technical University of Dresden. The governing and transport equations regarding heat and moisture transport solved by this simulation tool are described in detail in [5, 21]. For the purpose of the further discussion these equations are briefly repeated. However, the main emphasis of the present article lies in the air flow implementation in the current framework. The first part of this section discusses the complete set of balance equations in the porous media. The second part presents the corresponding transport equations.

2.1 Balance equations in porous media

The physical equations describing the combined heat and moisture transport in multilayered porous building components, documented during an European project (HAMSTAD [6]) are widely accepted and used in various publications [4, 16, 22, 23]. This set of partial differential equations is also solved in the simulation tool DELPHIN [5]. For the discussion that follows the conversation equation for energy and moisture mass are briefly repeated here (Eqn 1a and

1b):

$$\frac{\partial \rho^{w+v}}{\partial t} = -\nabla\left[j^v_{diff} + j^v_{conv} + j^w\right] \tag{1a}$$

$$\frac{\partial u}{\partial t} = -\nabla\left[q_{cond} + h_v\left(j^v_{diff} + j^v_{conv}\right) + h_w j^w + h_d j^d\right] + \Sigma \dot{u} \tag{1b}$$

$$\varphi \frac{\partial \rho^a}{\partial t} = -\nabla(\rho_a v_a) \tag{1c}$$

Here, u is the energy density (J/m^3), ρ a mass density (kg/m^3), q an energy/enthalpy flux (W/m^2), j a mass flux ($kg/m^2/s$) and $\dot{u}$ an energy source density (W/m^3). The superscripts w, v, a and d indicate liquid water, water vapour, humid air and the dry air components respectively. The subscripts describe the mode of transport through diffusion (*diff*) or convection (*conv*) and h_w, h_v and h_d are the specific enthalpies (J/kg) of the individual components considered. In contrast with liquid and dry air mass, the specific enthalpy of vapour consist of a sensible and latent part:

$$h_v = c_v\,(T - T_{ref}) + H_{evap} \tag{2a}$$

$$h_w = c_w\,(T - T_{ref}) \tag{2b}$$

$$h_d = c_d\,(T - T_{ref}) \tag{2c}$$

in which the corresponding levels of heat capacity are c_v=1840 J/kg/K, c_w=4180 J/kg/K and c_d=1006 J/kg/K, H_{evap}=2445 kJ/kg is the evaporation heat and T is the thermodynamic temperature (K).

The conservation of air mass in the porous medium is given in Eqn.1c according to [24] in which φ corresponds to the open porosity, ρ_a to the air density and v_a is the average velocity (so-called seepage velocity). For the envisaged applications the transient term on the left hand side of Eqn.1c can be questioned. Including the transient behaviour would allow to simulate the detailed dynamic evolution of the air transport, in direct interaction with moisture and temperature profiles. In this way specific effects such as the influence of air compression on the capillary moisture absorption rate can be captured [25]. However, the main goals of the current air flow implementation is the prediction of the hygrothermal response of building components over longer periods (up to several years). For such time scales, the mentioned effects become of minor importance. Furthermore, the transients of the air transport in building components is a few order of magnitude faster than these of heat and moisture transport. Air flow travels with nearly the speed of sound while the transients of heat and moisture transport can range from hours to months. As a result, the time derivative term in the left-hand side of Eqn. 1c can be safely omitted, and thus, air transport in building components can be modelled as a quasi steady-state phenomenon in combination with the transient heat and moisture transport [26, p.103]. Hence eq. simplifies to:

$$0 = \nabla(\rho_a v_a) = \nabla(j_a) \tag{3}$$

To increase the simulation performance some assumptions in the air properties can be made. The applied simplifications in the calculation of the air density, given in this section, are based on [27]. Humid air (a) is treated as a mixture of dry air (d) and water vapour (v) following the ideal gas equation:

$$\rho_i = \frac{p_i}{R_i\, T} \tag{4}$$

in which ρ_i represents the density of the component, p_i the partial pressure, R_i the gas constant and T the temperature. Thus, both components share the same volume and temperature of the mixture but have their individual partial pressure. The total pressure of the mixture follows from sum of the individual components according to Daltons law (Eqn. 5):

$$p_a = p_d + p_v \cong p_{atm} \tag{5}$$

For building physical applications the fluctuations of the air pressure are negligible against the total air pressure. As a result, a first simplification is to assume that the sum of partial pressures in Eqn. 5 equals the atmospheric air pressure (p_{atm} = 101325 Pa). Following from the ideal gas law (Eqn. 4), the total humid air density can be expressed as the sum of the water vapour density and the dry air density (Eqn. 6). This expression is rewritten in Eqn. 7 as a function of the total air pressure and the vapour pressure. In hygrothermal processes in building components the second term in Eqn. 7 is typically two to three orders of magnitude higher than the first, so the this term can be safely neglected. In this way, the air density is assumed to depend on the temperature only.

$$\rho_a = \frac{p_a - p_v}{R_d\, T} + \frac{p_v}{R_v\, T} \tag{6}$$

$$= \frac{p_a}{R_d\, T} - \frac{p_v}{T}\left(\frac{1}{R_d} - \frac{1}{R_v}\right) \cong \frac{p_{atm}}{R_d\, T} \tag{7}$$

Omitting the second term in Eqn. 7 becomes more important with higher temperatures. However, for exceptional temperatures of around 60°C, the air density is still only underestimated by less than 7%.

2.2 Heat and mass transport equations in porous domain

The heat transport consists of heat conduction and enthalpy fluxes of the mass transport. The latter are already given in Eqn.1b and are therefore not repeated here.The well-known transport equation for heat conduction, following Fourier's law, reads:

$$q_{cond} = -\lambda \nabla T \tag{8}$$

in which T the temperature (K) and λ the thermal conductivity (W/mK).

Moisture transport is induced by vapour and liquid water transport. Vapour transport consists of vapour diffusion (Eqn.9a) and vapour convection (9b). Liquid transport is also a convective process and is driven by capillary pressure (Eqn.9c).

$$j^{v}_{diff} = -\frac{\delta_a}{\mu_{w+v}} \nabla p_v \tag{9a}$$

$$j^{v}_{conv} = \frac{\rho_v}{\rho_a} j^{a} \tag{9b}$$

$$j^{w} = -K_w \nabla p_c \tag{9c}$$

For a detailed description of the heat and moisture transport equations we refer to [5].

The momentum equation in porous media is commonly expressed by the experimentally observed Darcy law [24].

$$v_a = -\frac{k_a}{\eta} \left(\nabla p_a + \rho_a \, g\right) \tag{10}$$

in which v_a is the seepage velocity, k_a corresponds to the air permeability (m^2), $\eta = 1.8 \times 10^{-5} \, Pa.s$ represents the dynamic viscosity and $g = 9.81 \, m/s^2$ is the gravity force. This phenomenological approach which neglects non-linear effects is justified for sufficiently low seepage velocities v_a. In this context, "sufficiently" small means that the Reynolds number Re_k of the flow, based on the square root of the permeability is of order unity or smaller [24]:

$$Re_k = \frac{v_a \sqrt{k_a}}{\nu} < 1 \tag{11}$$

where ν represents the kinetic viscosity. In this regime the viscous force dominates over the inertial force, so, only the local geometry or pore structure influences the flow behaviour. For building physical applications Re_k is far below this criterium, justifying the use of Darcy flow in the porous domain [9].

2.3 Boundary Conditions

This section gives a brief overview of the boundary conditions implemented in the DELPHIN simulation platform. Heat transport at the exterior boundary (Eqn. 12) consists of an imposed heat flux in which convective heat transfer, long-wave radiation and solar radiation are considered. Heat transfer at the interior boundary consists of a convective and long-wave radiation component (Eqn. 13).

$$q_e = \alpha_{ce}(T_e - T_{se}) + \alpha_{sw} q_{sw} + \alpha_{lw} q_{lw} \tag{12}$$

$$q_i = \alpha_i (T_i - T_{si}) \tag{13}$$

α_i is the interior heat exchange coefficient ($W/(m^2K)$), including both convective and long-wave radiation. T_i an T_{si}

are the interior air and interior surface temperature respectively (K), α_{ce} is the exterior convective exchange coefficient ($W/(m^2K)$), α_{sw} is the absorption coefficient for short wave radiation (-), q_{sw} the short-wave radiation heat flux (W/m^2), α_{lw} the emission coefficient for long wave radiation (-) and q_{lw} refers to the long waver radiation heat flux (W/m^2). Alternatively, for both the interior as the exterior also surface temperatures or surface heat flows can be imposed.

Surface air pressures are used as boundary condition for air transport. The driving forces for air flows through building enclosures are mechanical ventilation, stack effect and wind pressure. Consequently, these three phenomena determine the interior (Eqn. 15) and exterior (Eqn. 14) boundary conditions of building components.

$$p_e(z) = p_{e,ref} + \rho_e g\ (z_{ref} - z) + C_{p,e}\frac{\rho_e v^2}{2} \tag{14}$$

$$p_i(z) = p_{i,ref} + \rho_i g\ (z_{ref} - z) + \Delta p_{mech} + C_{p,i}\frac{\rho_i v^2}{2} \tag{15}$$

p correspondents with the total air pressure (Pa) and for simplicity index a is omitted here. Inner boundary conditions are referred with index i and the exterior conditions are defined by index e. The first term corresponds to the reference pressure. The second term refers to the hydrostatic pressure in which g refers to the gravity force. Pressure differences induced by mechanical ventilation are defined by Δp_{mech}. The last term in both the interior as the exterior pressure condition corresponds to wind pressure differences. Here, C_p is the surface wind pressure coefficient and v the local wind velocity (m/s).

Moisture exchange at the exterior boundary is defined by an imposed moisture flux in which convective vapour transfer and wind-driven rain are considered (Eqn. 16). Moisture flow at the interior boundary is imposed by a vapour transfer coefficient only (Eqn. 17):

$$j^{v+w}_{diff,e} = \beta_e(p_{v,i} - p_{v,si}) + j_{rain} \tag{16}$$

$$j^{v}_{diff,i} = \beta_i(p_{v,e} - p_{v,se}) \tag{17}$$

in which β corresponds to the vapour transfer coefficients, p_v and $p_{v,s}$ to the air and surface vapour pressures respectively and j_{rain} includes the moisture flow corresponding to wind-driven rain. The latter is limited to saturation conditions in the boundary layer and no run-off is included in the model. For more details on the boundary conditions we refer to [28].

3 Numerical implementation of the model

3.1 Spatial discretisation

In a first step the system of partial differential equations (PDE) is transformed into a set of ordinary differential equations (ODE) through discretisation. The Finite Volume Method (FVM) is used and the computational domain is subdivided in a number of finite volumes/elements resulting in discrete balance equations for all elements. The resulting spatial discretisation of the flux terms is done using the central-difference approximation for diffusion terms and upwinding schemes for the convective terms. For example suppose the left neighbour of element i is the element $i-1$ along the x-axis, with Δx_i and Δx_{i-1} as the respective element widths. The discretised forms of the heat conduction and enthalpy convection flux across interface $A_{L,i}$ between elements $i-1$ and i are given in Eqn. 18 and 19, respectively.

$$(q_{cond})_{L,i} = -\lambda_{L,i} \frac{T_i - T_{i-1}}{0.5\,(\Delta x_{i-1} + \Delta x_i)} \tag{18}$$

$$(h_a j^a)_{L,i} = \begin{cases} (h_a)_{i-1}\, j^a & j^a > 0 \\ (h_a)_i\, j^a & j^a \leq 0 \end{cases} \tag{19}$$

The transport coefficient λ is averaged using harmonic distance-weighted averaging between the elements which is again indicated through the subscript L, i.

3.2 Integration in time

With all spatial gradients replaced with finite difference approximations of the transient heat and moisture balance equations an ordinary differential equation system (ODE) is obtained. With the solution vector written as $y = \{\rho^U, \rho^{m_{w+v}}\}$, this system can be formally written as Eqn. 20:

$$\dot{y} = f\,(y, t) \tag{20}$$

in which $\dot{y}$ represent the time derivatives of the solution vector. In the current version of DELPHIN this system of combined and moisture transport is solved using a Newton-Raphson iteration method implemented in the generic ODE-solver from the SUNDAILS solver package [29]. The implementation of this generic multi-step solver in the DELPHIN framework is extensively documented in [5]. However, since the air mass balance equation is simplified to a steady state formulation, its discretised form can not be included in the general form of Eqn. 20. Therefore, this set of linear equations is solved separately from the coupled transient heat and moisture transport. In respect the quasi-steady state implementations means that during integration of the coupled energy and moisture balance equations the air flow field is kept constant. At defined time intervals a new steady-state solution of the air flow field is calculated

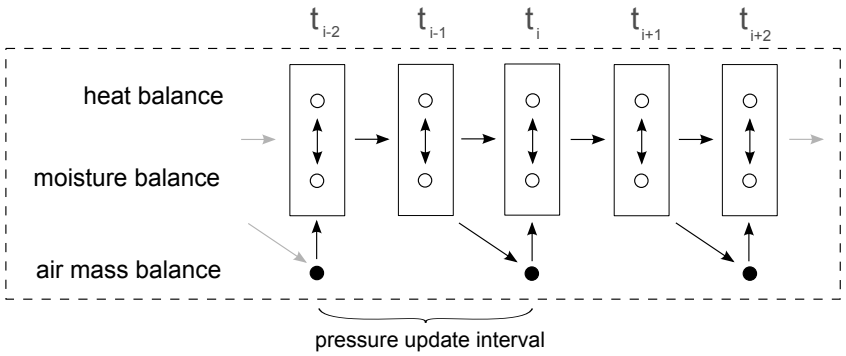

Figure 2: Integration schematics for computation of quasi-steady air flow field and transient energy and moisture balances

and used during the continued integration of heat and moisture balances as depicted in Figure 2.

In forced convection scenarios the air flow field is largely depending on the change of boundary pressures, which are commonly available as hourly weather data. The air flow field changes only very rapidly within the first few seconds after a new pressure condition is applied. For the remainder of the hour it will be constant. Thus, it can be argued that considering the effect of air flow on energy and moisture balance, the first few seconds can be safely taken to be the same as during the remainder of the hour. As a result a steady-state air flow field can be calculated whenever boundary pressures change and be kept constant during the calculation of energy and moisture balance. This calculation method essentially decouples air balance from energy and moisture balances which improves simulation performance significantly. For forced convection scenario this assumption is relevant since there is no direct coupling term between the air and heat balance equations. However when applying this method to buoyancy dominated simulation problems, the pressure field becomes affected by the temperature distribution as the density in the second term of the right hand side of Eqn. 10 couples the energy and air mass balance equations. Given the decoupled solution method it is advised to increase the air pressure calculation, so it will be updated after each time step of the integration of the heat and moisture balance equations. This is addressed more in detail and illustrated with an example in section 4.2.2. In order to investigate the applicability of the proposed integration strategy the next section mainly focusses on the evaluation of its accuracy in simulating heat and moisture transport in combination with overlaying natural convection.

4 Validation of the numerical Heat, Air and Moisture model

The current section confronts the numerical simulation tool with analytical, numerical and laboratory results from the literature. The combined heat and moisture transport of the model (DELPHIN 5) is already extensively validated in the framework of the EU-initiated HAMSTAD (Heat, Air and Moisture Standards Development) project [16, 23, 30]. As a consequence the main focus of present validation is on the impact of air convection on the heat and moisture response. In particular the interest lies in the effects of natural convection since this implies a coupling between the heat and air balance equations through the density of air (second term in Eqn. 10). The first two validation cases study

free heat convection in porous media. The first project focusses on steady-state conditions, while the second evaluates the predication of the transient behaviour. In a final step the model is compared with laboratory results studying the effects of air convection on the hygrothermal behaviour of a timber framed wall.

4.1 Steady state free convection in a vertical and horizontal insulation layer

The first case investigates the two dimensional steady state natural convection through a vertical and horizontal positioned insulation layer. This topic is well documented in the literature by theoretical and experimental results in the field of building physics such as [e.g. 31–33]. Consequently, the thermal performance of a porous insulation layer is a straightforward first step in evaluating the model. This validation project, investigated by Kohonen [34] and also applied and documented by Janssens [9], consists of an anisotropic glass fibre layer of 2.2m by 0.3m. The imposed interior surface temperature is 20°C and the exterior surface temperature is −20°C resulting in a temperature difference ΔT of 40°C across the wall. A hydrostatic pressure along both the exterior and interior boundary is assumed. The warm surface is supposed airtight while the cold surface is either airtight or air open. Both short boundaries are adiabatic and impermeable. As a result of internal buoyancy, additional heat losses occur as function of the air permeability of the insulation layer. The Nusselt number (Nu) quantifies this effect as the ratio of the heat loss through the structure to the total heat loss by conduction only (Eqn.21). Figure 3 plots the computed Nusselt numbers as function of the dimensionless Darcy-modified Rayleigh number (Ra_D) to include the anisotropicity of the material [31].

$$Nu = \frac{Q_{tot}}{Q_{cond}} = \frac{Q_{tot}}{H\Delta T(\lambda_x/D)} \tag{21}$$

$$Ra_D = g\beta D\Delta T\Big(\frac{\rho c}{\nu}\Big)\frac{k_x}{\lambda_x}\frac{4a_k}{(\sqrt{a_\lambda}+\sqrt{a_k})^2} \tag{22}$$

in which Q_{tot} represents the total heat flux through the porous layer as result of both conduction and natural convection, Q_{cond} is the heat flux including conduction only, H and D are the height and width of the layer. Furthermore β represents the thermal expansion coefficient of air ($3.7\,10^{-3}1/K$), ν the kinematic viscosity of air ($1.4\,10^{-5}m^2/s$), k_x is the air permeability (m^2) in the x-direction and a_k=1.875 and a_λ=1.021 are the anisotropicity ratios of the air permeability and the heat conductivity respectively. Simulations are made using an equidistant 20 by 20 grid.

The current model has been validated for both the vertical and horizontal porous layer. The simulations are conducted with the cold surface either permeable or impermeable. Figure 3a shows the results of the vertical layer and compares it with the analytical solution of Weber and the numerical results of Janssens [9]. Good agreement is found between the different models and the analytical solution.

Figure 3b summarises the results of the simulation of the horizontal layer heated from below. In contrast with the vertical insulation layer the heat flux only starts to increase when a critical Ra_D is reached. For impermeable surfaces the critical Ra_D is $4\pi^2 \approx 39.5$, for a permeable cold surface and a isotropic media this threshold value is 27.1 [35].

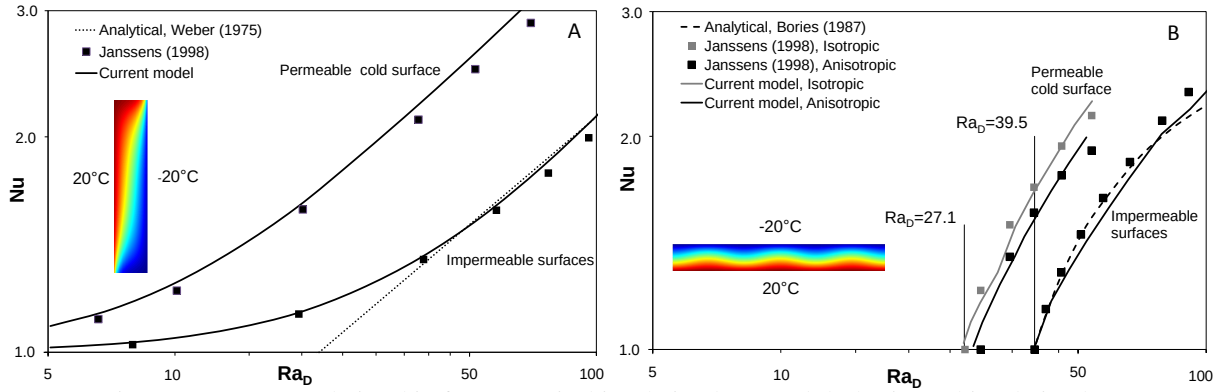

Figure 3: $Nu(Ra_D)$ relationship for (a) vertical insulation layer and (b) horizontal insulation layer

Above the critical Ra_D buoyancy loops (known as Bénard-cells) develop, resulting in an increased heat flux. Figure 3b shows that the critical Ra_D predicted with the present model is consistent with the mentioned theoretical values from the literature. In addition this figure shows that the simulations with both surfaces airtight are in good agreement with the analytical solution of Bories and the numerical results of Janssens [9]. The same applies for the results of the anisotropic and isotropic variants of the permeable cold boundary which are only compared with the results of Janssens [9]. Furthermore, it has to be noticed that normal building component correspond to Ra_D numbers lower than 10, even in extreme climate conditions. Consequently it can be stated that present model is sufficiently accurate for the proposed range of purposes.

4.2 Transient free convection in a cavity filled with a porous medium

The previous section showed the models capability to predict free convection in a vertical and horizontal porous layer under steady state conditions. However, since the heat and air equations are basically decoupled in the presented model, the main interest lies in its reliability for the prediction of transient HAM-behaviour. As logical next step the current section investigates the models ability to capture transient free convection. Detailed studies regarding transient natural convection are scarce, if not nonexistent in the field of building physics. As a consequence a more general validation project from the field of heat and mass transfer described by Saied [36] is selected at first. This validation case corresponds to an abstract configuration instead of a typical building component. However, for the purpose of validating the transient behaviour of natural convection in a porous media this is of minor importance.

The second part of this section illustrates the importance of the frequency with which the air flow field updated. This will be investigated on the basis of the vertical insulation layer of the previous section to which an fluctuating boundary temperature will be applied.

4.2.1 Validation

Description of validation project Saied [36] studied transient free convection in a two-dimensional square cavity (side = L) filled with an isotropic porous medium (Figure 4). The initial uniform temperature of the cavity is $T_0 = (T_h + T_c)/2$. The left vertical wall is suddenly heated to a constant temperature T_h, while the right wall is cooled to a constant temperature T_c by equal amount relative to the initial temperature. Both horizontal walls are adiabatic. Saied [36] rewrites the governing equations in a non-dimensional form, which are then numerically solved with a finite volume method based on convection-diffusion formulation of Patankar [37].

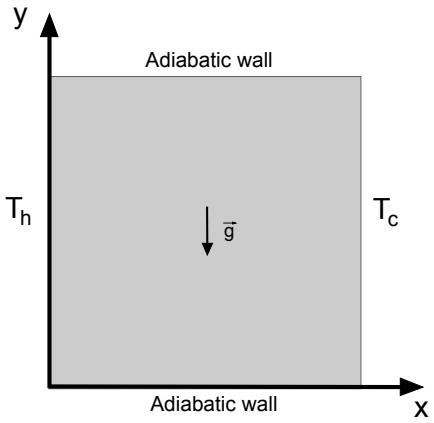

Figure 4: Configuration of the phyiscal model and coordinate system [36]

The physical quantity of interest is the average Nusselt number ($\overline{Nu}$) along the warm wall as a function of the non-dimensional time τ, defined by:

$$\overline{Nu} = \int_0^1 (-\frac{\partial \theta}{\partial X})_{X=0}\, dY \qquad with \quad X = \frac{x}{L}, Y = \frac{y}{L} \tag{23}$$

$$\tau = \frac{\lambda t}{\rho c \sigma L^2} \tag{24}$$

in which σ corresponds to the ratio of composite material heat capacity to convective fluid heat capacity.

Simulation set-up and numerical results In order to simulated the discussed non-dimensional validation case with the present model it is necessary to define its size and assign material properties and boundary conditions. The sides of the cavity are assumed to be 1m. Standard mineral wool (λ=0.035 W/m^2/K, ρ=20 kg/m^3 and c=840 J/kg/K) is applied as porous medium. In accordance with the validation project the porous medium is isotropic. The hot wall has a temperature of 10 °C and the cold wall has a temperature of -10°C. The air permeability k is 6 10^{-8} m^2, so the current configuration corresponds to a Rayleigh number of 100. Saied gives the results for Rayleigh numbers ranging from 100 to 10 000. However, as discussed in section 4.1 the order of magnitude of Rayleigh numbers of building components is around 10. Consequently the lowest Ra number available in the benchmark of Saied (Ra=100) is chosen. This is still ten orders of magnitude higher, so, if the present model satisfies this benchmark it can be safely

used for lower Rayleigh numbers as well.

In accordance with [36] a non-uniform grid of 41x41 elements is used such that the grid points are clustered near the walls. Furthermore, it is important to notice that the air flow calculation was updated after each time step of the integration of the heat balance equation. Figure 5 compares the simulation results of the present model with the results from [36]. The figure shows that present model is in very good agreement with the benchmark results. This means that the decoupled integration strategy is capable the capture transient free heat convection. Next section investigates the importance of the update intervals of the airflow field and illustrate the simulation performance of the present model for a more realistic configuration.

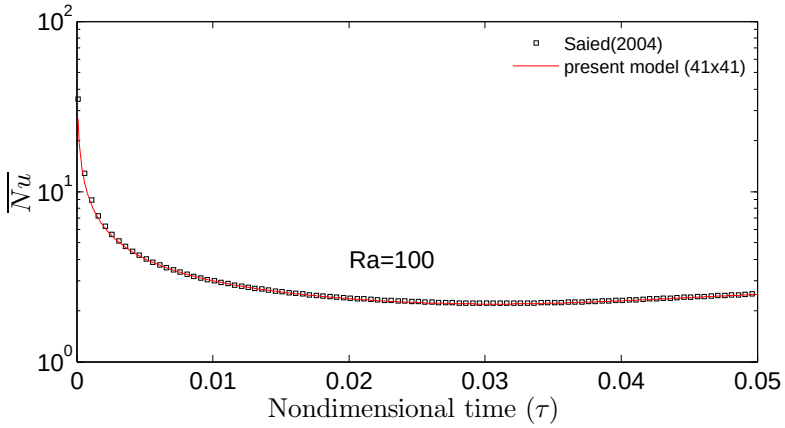

Figure 5: Evolution of the transient average Nusselt number as a function of the dimensionless time (τ) for Ra=100

4.2.2 Pressure update intervals and simulation performance

The current section investigates the impact of the pressure field update interval during the integration of the heat balance equation. The configuration applied in this study corresponds to the vertical insulation layer of section 4.1. However, instead of constant exterior temperature, a cosine function with a period of one day, an amplitude of 10°C and a mean value of -10°C is imposed. The interior temperature on the other hand, is kept at 20°C and the initial temperature is also 20°C. The temperatures are imposed as surface values and the both sides are assumed airtight. Furthermore, the same mineral wool as in section 4.2.1 is used for the simulation. Only the air permeability of the insulation layer (k_x) was adjusted to 3.6 10^{-8} m^2, so that the Darcy-modified Rayleigh number (Ra_D) equals 50. This periodical situation was simulated for three days and the boundary conditions were imposed on an hourly basis (which is most common in HAM-modelling). The simulation was performed using an variable distance grid with 27 by 27 nodes.

The simulations were repeated, varying the update interval of the air flow calculation. Figure 6 shows the total heat flux at the interior surface for three different update intervals. Furthermore, this figure also includes the simulation in which air transport is excluded. The average step size for decoupled simulation was around 5 minutes. It was found that when the update interval lies between an update after each time step and an hourly update, the simulation

results are identical. In addition, to illustrates the error when applying larger updates intervals, the figure also plots the simulation results corresponding to an 6-hourly update of the pressure field. Figure 6 shows that these simulation results only corresponds to the correct solution short after an update of the air flow field.

Notwithstanding the present example indicates that larger update intervals (up to one hour) can be used, it is suggested to update the airflow calculation after each time step of the heat and moisture integration. The additional calculation time of updating the pressure field is relatively small against the integration of heat and moisture balance equations. Only when the time steps of the heat and moisture calculation become very small (e.g. for water absorption as result of wind driven rain) larger update intervals of the pressure field become interesting to avoid superfluous calculations, and thus, increase simulation times.

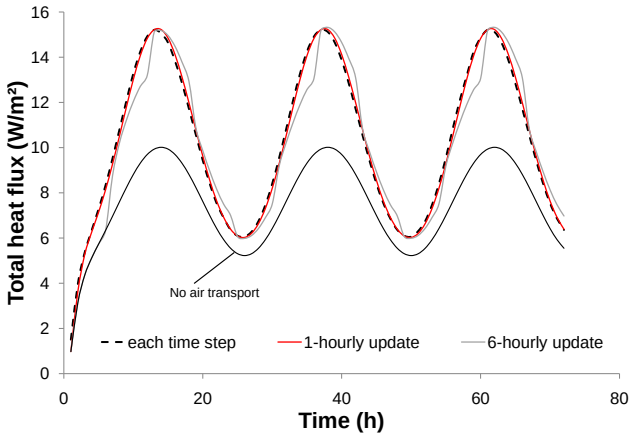

Figure 6: Total heat flux at the interior surface for different pressure update intervals

To compare the simulation performance of the decoupled strategy, the simulation was also repeated with a fully coupled solution of the air and heat balance equations (Eqn. 3 and 1b). For this coupled simulation the DAE[1]-solver from the SUNDAILS generic solver package is applied [38]. This solver has similar performance properties as the ODE-solver which is used in the decoupled approach. However, the DAE-integrator allows to solve the given set of differential-algebraic equations in coupled way.

Firstly, the additional simulation results in the same heat flow profile as depicted in Figure 6. Only small deviations (<3%) near the upper values were found between the results, confirming again the accurate results of the decoupled calculation. Secondly, the additional simulation showed that the decoupled strategy might lead to better simulation performances. When only the heat balance equation is solved, the DAE-solver is slightly faster, proving that the overall performance of both solvers is similar. However, when including air transport the coupled simulation was around ten times slower than the decoupled strategy (even with a pressure update after each time step). This indicates the potential advantage of shorter simulation times for the decoupled approach. However, in order to draw general conclusions in this respect, the solver performances have to be studied more in depth which falls outside the scope of this article.

[1]Differential-Algebraic Equations

4.3 Impact of air convection on the hygrothermal response of a timber frame wall

The first two validation cases in sections 4.1 and 4.2.1 confronted the present model to analytical and numerical results from the literature. The results show the models ability to capture the coupled phenomena of free heat convection. However, the main interest of developing the model lies in the prediction of combined heat, air and moisture transfer in building components. Therefore, in a third step the model is confronted with a well-controlled laboratory investigation studying the effect of air convection on the hygrothermal behaviour of a timber frame wall. Langmans [39] performed a comprehensive investigation to study the effect of exterior air barriers. The tests are conducted with high accuracy and with the objective to create two dimensional conditions which make them very suitable for evaluating the present model.

4.3.1 Brief description of the laboratory tests and simulation set-up

The test setup is only very briefly discussed here. More details on the configuration, material properties and results can be found in [39]. Four test walls (each 2.3m by 0.5m) are placed between a hot and cold box, operating at controlled temperatures, humidity levels and air pressures. Only one test wall is simulated here (referred to as Fibreboard 1 in [39]). The test wall is insulated with 30 cm mineral wool to which OSB is applied as interior vapour retarder. At the outer side a bituminous mixed wood fibreboard is applied as sheathing material. The experiment, which lasted about four months, was subdivided in five main consecutive measuring steps. An overview of the corresponding boundary conditions is given at the top of Figure 9. In the first four steps the test wall was exposed to typical Belgium winter conditions. During the first step, both the interior and exterior sheathing is airtight. In the second step, gaps are introduced in the interior barrier. The gaps correspond to slots of 1 cm at 20 cm from the top and bottom of the OSB and extend the full width of the test wall to maintain the two dimensional situation. In step 3 and 4 the hot box was pressurised to 6 Pa and 11 Pa respectively. Finally, in the last step the conditions in the cold box were adapted to create drying conditions inside the wall. The configuration of this test wall is presented in Figure 7. In this figure the position of the temperature and relative humidity sensors of interest for the current validation are presented as red dots. Apart from the sensors also three removable weight specimens are integrated in the exterior barrier.

The experimental data set is used for the verification of the presented model. For the simulation the calculation domain was discretized in 1484 cells (28x53) using a variable distant grid with refinements at the gaps height and near the interfaces. The measured temperature, relative humidity and air pressure at the cold and warm boundary at the mid height are applied as boundary conditions for the simulations. The measured boundary air pressures ascribed to the model are adjusted over the height with the hydrostatic air pressure based on the measured temperature at both sides. The boundary conditions were applied as hourly data in the transient simulation and the material properties are adopted from [39].

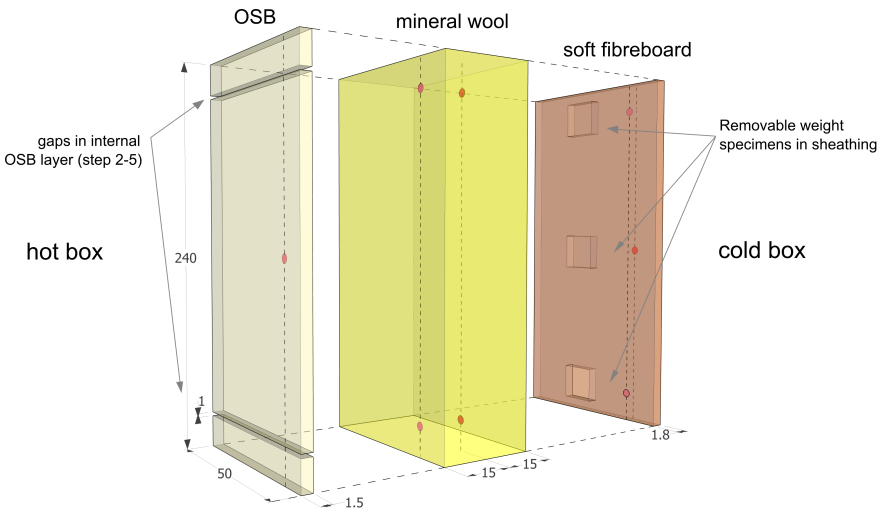

Figure 7: Expanded view of test wall (cm). Red dots indicate the positions of the temperature and relative humidity sensors

4.3.2 Comparison between measured and simulated temperature and vapour pressure profiles

To illustrate the impact of air convection on the hygrothermal behaviour of the wall Langmans [39] presents the dimensionless temperature and vapour pressure profiles during the different measuring steps. The profiles are given for the top and bottom row (Figure 7) to visualise the effect of natural convection. This figure is selected for comparison with the simulation results. Figure 8 shows the non-dimensional temperature and vapour pressure profile of both the measured data and the simulations for the situations where (1) the interior OSB sheathing is intact, (2) top and bottom gaps in the interior sheathing are introduced and (3) an overpressure of 11 Pa is realised in the warm chamber. The simulated profiles are represented as lines and the measured profiles with markers. Full lines and markers correspond to temperatures and vapour pressures at the top position and dotted lines and hollow markers to these of the bottom position. The first measuring step is coloured in blue, the second in red and the fourth step in green.

During the first step the measuring data (blue) clearly shows that the temperature distribution bends upwards at the top (filled markers) and downwards at the bottom (open markers) indicating the existence of natural convection within the walls. This is confirmed by the simulations, which show an identical profile. During the second measuring step (in red) the effect of natural convection on the temperature profile increases as a result of introducing gaps in the interior sheathing. When finally an overpressure of 11 Pa (in green) is realised in the fourth step a slight increase of the temperature is noticed as a result of forced convection. Overall, it can be concluded that the simulation results predict the same trends as the measuring data. Since the simulated temperatures at the upper cold side and middle of the insulation are lower than the measured temperatures it can be concluded that the simulations slightly underestimate the effect of natural convection. This can be explained by inevitable small gaps at the interface of the insulation layer and the exterior sheathing in the measured walls. Brown [40] shows that even very small air gaps around the insulation batts locally reduce its air permeability, and thus increase the effect of natural convection. In the simulation on the other hand, ideal contact between the insulation and adjacent layers is assumed which can explain the observed

discrepancies.

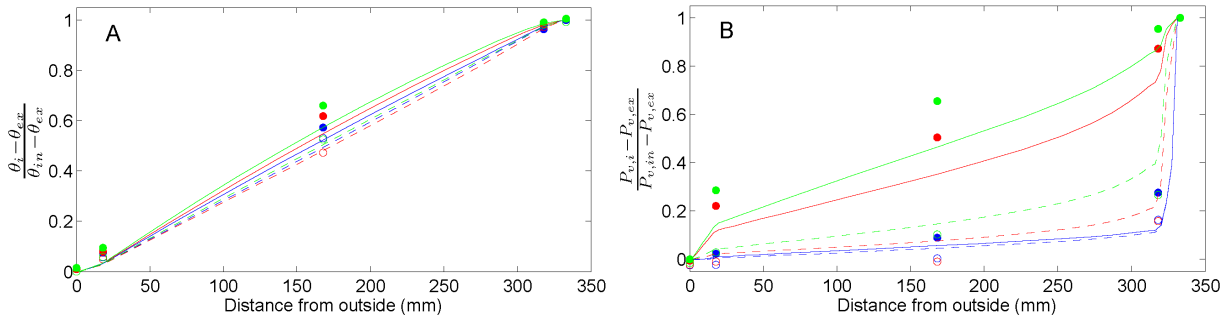

Figure 8: Comparison of the simulations against the measurement: (A) temperature profile and (B) vapour pressure profile across the wall at top and bottom row (Colours: step 1 in blue, step 2 in red, step 4 in green. Filled marker: top row and Hollow markers: bottom row)

Figure 8b compares in the same way the simulated vapour profiles with the measured data. During the first step (blue) the measured data shows a similar vapour pressure profile: steep drop behind the vapour retarder (OSB) followed by a slight decrease towards the outer side. In the subsequent step (red), when the gaps in the interior sheathing are opened, the influence of natural convection on the moisture load becomes very pronounced. For this situation both the measurements and the simulations indicate that the vapour pressure at the top row increases while the vapour pressure at the bottom row remains the same. When finally an overpressure of 11 Pa is realised the vapour pressure profiles slightly increase as a result of forced exfiltration. Again the simulations show the same trend as the measuring data. Quantitatively however, the vapour pressures at the upper cold and middle part of the insulation are underestimated by the simulation. The omission of air leakages in the simulation, as mentioned above, can partly explain these difference. Other possible explanations for these small discrepancies are uncertainties in the hygric material properties of the exterior sheathing. Roels [41] showed that surely for the vapour permeance high uncertainties can be expected.

4.3.3 Comparison between measured and simulated moisture content profile of the exterior sheathing

Figure 7 showed how three removable weight specimens are installed in the exterior sheathing material to follow the moisture evolution in this layer. These weights, measured on a two-weekly basis, are compared with the simulated moisture contents in Figure 9. Here, the measured weights are represented as filled markers and the simulated values are shown as continuous lines as explained in the associated legend. The top, mid and bottom height corresponds to black, red and blue respectively. The figure shows that from the moment gaps are introduced in step 2, the measured moisture content at the top position starts to increase up to 0.18 kg/kg at the end of step 4. At the same time the moisture content at the mid and bottom position are not influenced by the gaps in the interiors sheathing. The simulations follow the same trend. When drying conditions are applied in the final step the exterior sheathing dries out rapidly as a result of its high vapour diffusivity. Although the moisture content profiles deviates by more than 10% at the end op step 4, it can be concluded that the major effects of combined forced and natural convection are captured by the model. The

differences between the measurement and the simulation are in the order of magnitude of the accuracy in determining the material properties.

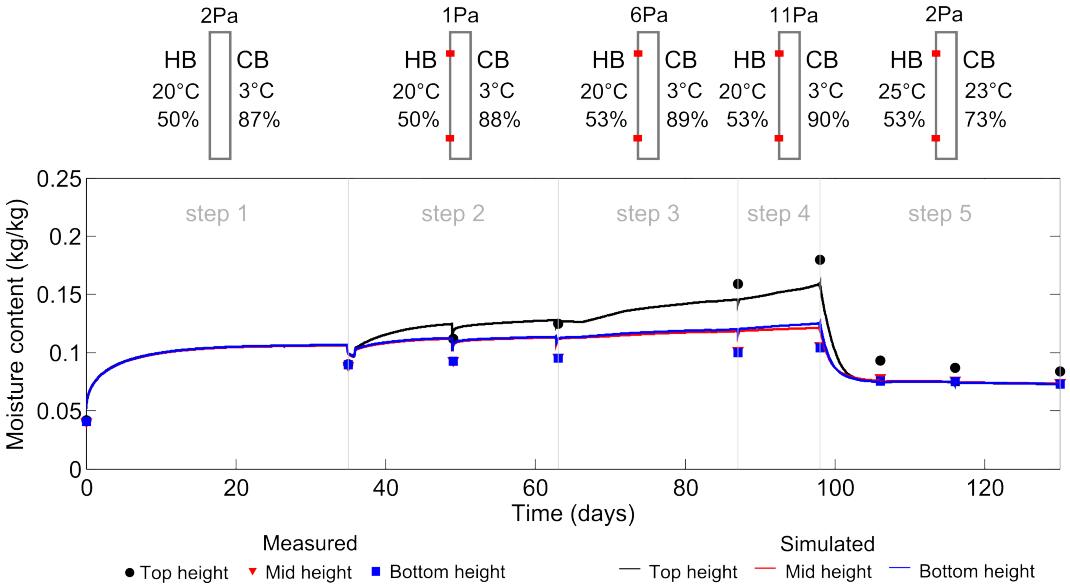

Figure 9: Confrontation of the simulated moisture contents against the measurement.

5 Conclusion

The current article presents the results of a quasi-steady state airflow implementation in the framework of an existing transient HAM-model for building components. The first section discusses the applied balance equations, transport mechanisms and the numerical strategy. The air transport is described as Darcy flow in porous media including a body force term to capture natural convection.

As a result of the different times scales between the combined heat and moisture transport and air transport, the paper shows that it is justified to neglect the transient effects of air transport. Moreover, the air mass balance equation could be solved externally to improve simulation performance.

The second part of the paper confronts the presented model with analytical, numerical and laboratory results from the literature. Three two-dimensional benchmark cases are used: (1) steady-state heat convection through a vertical and horizontal porous medium, (2) transient heat convection through a porous media, (3) transient heat, air and moisture transport in a light weight building wall. The first validation case shows the models capacity to predict the increased heat transport through light weight building components induced by natural convection. Both the results of the vertical wall as well as the unstable phenomenon of heat flow through a horizontal porous media heated from below are in good agreement with the results from the literature. The second benchmark proofs that the decoupled calculation approach is justified for building physical applications. For Ra-numbers lower than 100 the transient free heat convection is correctly predicted. Since the final validation project corresponds to experimental laboratory results, higher

deviations between the measurement and the simulation were noticed. Nevertheless, the overall trends in the simulated temperature, vapour pressure and moisture evolution were in good agreement with the measuring data.

Acknowledgment

Research funded by a Ph.D. grant (grant number 81153) of the Institute for the Promotion of Innovation through Science and Technology in Flanders (IWT-Vlaanderen).

References

[1] H. Janssen, *The influence of soil moisture transfer on building heat loss via the ground*. PhD thesis, Catholic University of Leuven, Departement of Civil Engineering, July 2002.

[2] H. M. Künzel, "Simultaneous Heat and Moisture Transport in Building Components: One- and two-dimensional calculation using simple parameters," tech. rep., Fraunhofer IRB Verlag Stuttgart, 1995.

[3] C. Rode Pedersen, *Combined heat and moisture transfer in building constructions*. PhD thesis, Technical University of Denmark, Lyngby, 1990.

[4] G. H. dos Santos and N. Mendes, "Combined Heat, Air and Moisture (HAM) Transfer Model for Porous Building Materials," *Journal of Building Physics*, vol. 32, pp. 203–220, Jan. 2009.

[5] A. Nicolai, *Modelling and numerical simulation of salt transport and phase transitions in unsaturated porous building materials*. PhD thesis, Syracuse University, Departement of Mechanical Engineering, 2007.

[6] C. E. Hagentoft, A. S. Kalagasidis, B. Adl-Zarrabi, S. Roels, J. Carmeliet, H. Hens, J. Grunewald, M. Funk, R. Becker, D. Shamir, O. Adan, H. Brocken, K. Kumaran, and R. Djebbar, "Assessment Method of Numerical Prediction Models for Combined Heat, Air and Moisture Transfer in Building Components: Benchmarks for One-dimensional Cases," *Journal of Thermal Envelope and Building Science*, vol. 27, pp. 327–352, Apr. 2004.

[7] N. B. Hutcheon, *Humidified buildings*. Canadian Building Digest, 1963.

[8] M. Z. Rousseau, "Control of surface and concealed condensation," in *building Insight '83*, 1993.

[9] A. Janssens, *Reliable Control of Interstitial Condensation in Lightweight Roof Systems: Calculation and Assessemnt Methods*. PhD thesis, Katholieke Universiteit Leuven, 1998.

[10] D. Derome, "Moisture Accumulation in Cellulose Insulation Caused by Air Leakage in Flat Wood Frame Roofs," *Journal of Thermal Envelope and Building Science*, vol. 28, pp. 269–287, Jan. 2005.

[11] T. Kalamees and J. Kurnitski, "Moisture Convection Performance of External Walls and Roofs," *Journal of Building Physics*, vol. 33, pp. 1–23, Aug. 2009.

[12] T. Z. Desta, J. Langmans, and S. Roels, "Experimental data set for validation of heat, air and moisture transport models of building envelopes," *Building and Environment*, vol. 46, pp. 1038–1046, May 2011.

[13] D. Zirkelbach, H. M. Künzel, and B. Schafaczek, "Dampfkonvektion wird berechenbar – Instationäres Modell zur Berücksichtigung von konvektivem Feuchteeintrag bei der Simulation von Leicht- baukonstruktionen," in *4th International Symposium on Building and Ductwork Airtightness & 30th AIVC Conference*, (Berlin), pp. 1–8, 2009.

[14] T. Ojanen, R. Kohonen, and M. K. Kumaran, "Modeling heat, air, and moisture transport through building materials and components," in *Moisture control in buildings* (H. R. Trechsel, ed.), ch. 2, ASTM International, 1994.

[15] H. R. Trechsel, *Moisture Analysis and Condensation Control in Building Envelopes: (MNL 40)*. ASTM International, 2001.

[16] Q. Li, J. Rao, and P. Fazio, "Development of HAM tool for building envelope analysis," *Building and Environment*, vol. 44, pp. 1065–1073, May 2009.

[17] H. H. Saber, M. C. Swinton, P. Kalinger, and R. M. Paroli, "Long-term hygrothermal performance of white and black roofs in North American climates," *Building and Environment*, vol. 50, pp. 141–154, Apr. 2012.

[18] A. W. M. van Schijndel, "Modeling and solving building physics problems with FemLab," *Building and Environment*, vol. 38, pp. 319–327, Feb. 2003.

[19] H.-J. Steeman, M. V. Belleghem, A. Janssens, and M. D. Paepe, "Coupled simulation of heat and moisture transport in air and porous materials for the assessment of moisture related damage," *Building and Environment*, vol. 44, no. 10, pp. 2176–2184, 2009.

[20] T. Defraeye, B. Blocken, and J. Carmeliet, "Analysis of convective heat and mass transfer coefficients for convective drying of a porous flat plate by conjugate modelling," *International Journal of Heat and Mass Transfer*, vol. 55, pp. 112–124, Jan. 2012.

[21] J. Grunewald, *Diffusiver und konvektiver Stoff- und Energietransport*. PhD thesis, University of Technology Dresden, 1997.

[22] H. Janssen, B. Blocken, and J. Carmeliet, "Conservative modelling of the moisture and heat transfer in building components under atmospheric excitation," *International Journal of Heat and Mass Transfer*, vol. 50, pp. 1128–1140, Mar. 2007.

[23] F. Tariku, K. Kumaran, and P. Fazio, "Transient model for coupled heat, air and moisture transfer through multi-layered porous media," *International Journal of Heat and Mass Transfer*, vol. 53, pp. 3035–3044, July 2010.

[24] D. Nield and A. Bejan, *Convection in porous media*. Springer-Verslag New York, 3rd ed., 2006.

[25] F. Descamps, *Continuum and discrete modelling of isothermal water and air flow in porous media*. PhD thesis, Catholic University of Leuven, 1996.

[26] H. Hens, A. Janssens, W. Depraetere, J. Carmeliet, and J. Lecompte, "Brick Cavity Walls: A Performance Analysis Based on Measurements and Simulations," *Journal of Building Physics*, vol. 31, pp. 95–124, Oct. 2007.

[27] H. Janssen, *Thermal performance of highly insulated wood frame walls*. PhD thesis, 1997.

[28] A. Nicolai, "Delphin 5, Numerical simulation tool for the coupled heat, air, moisture and salt transport, Webpage, \textit{http://www.bauklimatik-dresden.de/delphin5}," 2007.

[29] A. Hindmarsh, "SUNDIALS:Suite of Nonlinear and Differnential/Algebraic Equations Solvers.," tech. rep., 2005.

[30] C.-E. Hagentoft, "HAMSTAD: WP2: Benchmark package," tech. rep., University of Technology, Chalmers, 2002.

[31] S. Klarsfeld and M. Combarnous, "Analyse des transferts thermiques convectifs dans les isolants poreux perméables," *Revue generale de thermique*, vol. 228, 1980.

[32] F. Powell, M. Krarti, and A. Tuluca, "Air Movement Influence on the Effective Thermal Resistance of Porous Insulations: A Literature Survey," *Journal of Building Physics*, vol. 12, pp. 239–251, Jan. 1989.

[33] A. Silberstein, C. Langlais, and E. Arquis, "Natural Convection in Light Fibrous Insulating Materials with Permeable Interfaces: Onset Criteria and Its Effect on the Thermal Performances of the Product," *Journal of Building Physics*, vol. 14, pp. 22–42, July 1990.

[34] R. Kohonen, E. Kokko, O. T., and V. M., "Thermal effects of air flows in building structures," tech. rep., Technical Reserach Centre Finland, VTT Espoo. Research reports 367, 1985.

[35] A. Bejan, *Convection heat transfer*, vol. Third. John Wiley & Sons, New Jersey, 2004.

[36] N. H. Saeid and I. Pop, "Transient free convection in a square cavity filled with a porous medium," *International Journal of Heat and Mass Transfer*, vol. 47, no. 8-9, pp. 1917–1924, 2004.

[37] S. V. Patankar, *Numerical heat transfer and fluid flow*. Series in computational methods in mechanics and thermal sciences, Washington: Hemisphere, 1980.

[38] J. Langmans, A. Nicolai, R. Klein, G. J., and S. Roels, "Numerical Simulation of Building Components - Towards an Efficient Implementation of Air Convection in HAM-models," in *9th Nordic Symposium on Building Physics*, (Tampere,Finland), pp. 399–405, Tampere University of Technology, 2011.

[39] J. Langmans, R. Klein, and S. Roels, "Hygrothermal risks of using exterior air barrier systems for highly insulated light weight walls: a laboratory investigation," *Building and Environment*, vol. 56, no. 10, pp. 192–202, 2012.

[40] W. C. Brown, M. T. Bomberg, J. M. Ullett, and J. Rasmussen, "Measured Thermal Resistance of Frame Walls with Defects in the Installation of Mineral Fibre Insulation," *Journal of Building Physics*, vol. 16, pp. 318–339, Apr. 1993.

[41] S. Roels, P. Talukdar, C. James, and C. J. Simonson, "Reliability of material data measurements for hygroscopic buffering," *International Journal of Heat and Mass Transfer*, vol. 53, pp. 5355–5363, Nov. 2010.